Deep–Sea Research I 164 (2020) 103308

Contents lists available at ScienceDirect

Deep-Sea Research Part I

journal homepage: http://www.elsevier.com/locate/dsri

# The Zapiola Anticyclone: A Lagrangian study of its kinematics in an eddy-permitting ocean model

Wilbert Weijer [a,*], Alice Barthel [a], Milena Veneziani [a], Hannah Steiner [b,1]

[a] Los Alamos National Laboratory, Los Alamos, NM, USA
[b] United States Naval Academy, Annapolis, MD, USA

ARTICLE INFO

*Keywords:*
Zapiola anticyclone
Argentine basin
Lagrangian particle tracking

ABSTRACT

The Zapiola Anticyclone (ZA) is a strong, ∼(100 Sv), barotropic vortex in the center of the Argentine Basin that is tied to a bathymetric feature called the Zapiola Rise. It is regionally significant for two reasons: first, the strong vortex is a dynamical barrier that inhibits the lateral exchange of water, and hence has the ability to trap water for a long period of time. Second, its dynamics is governed by a balance between eddy-driven mass convergence and divergent Ekman transport, which gives rise to strong downwelling and Ekman pumping into the bottom boundary layer.

This study investigates the kinematics of the ZA by studying the fate of the water parcels that are trapped by the ZA. We use output from a five-year simulation with an eddy-permitting ocean model, and we use a Lagrangian approach to track water parcels originating from within the ZA. We determine basic statistics of the parcel trajectories, including retention time, number of revolutions, vertical displacement, and temperature and salinity changes. The picture that emerges is one of water parcels spiraling downward through the water column, undergoing downwelling while they revolve anticyclonically around the center of the ZA. In our experiment, water parcels spend on average 451 days within the ZA, and make 2.6 revolutions around its center, with each revolution taking somewhere between 100 and 200 days. On average, parcels undergo a 94 m descent, 0.03 °C cooling and 0.0042 psu freshening. But individual parcels can undergo more than 800 m of downwelling, 0.2 °C of cooling, and ± 0.02 psu of salinity change. We believe that vertical motions of this order of magnitude, and the associated water mass transformations, are unique in the abyssal mid-latitude oceans.

## 1. Introduction

The Zapiola Anticyclone (ZA) is a stationary vortex located in the Argentine Basin. It is trapped by a seamount called the Zapiola Rise, which crests at 4700 m depth and rises 1500 m above the Argentine Abyssal Plain (Fig. 1). The ZA is roughly 800 km wide, and is barotropic in nature (Saunders and King, 1995a). Its mean volume transport is not well constrained, due to the difficulty of measuring barotropic transports, and the strong variability in the region; and it seems that the only direct observation was made by Saunders and King (1995a), who estimated a strength of 100 Sv (1 Sv $\equiv 1{\cdot}10^6\ m^3\ s^{-1}$) based on Acoustic Doppler Current Profiler (ADCP) measurements. Subsequently, Saraceno et al. (2009) estimated a strength of about 50 Sv based on the Mean Dynamic Topography (MDT) product of Rio et al. (2005) –which combined gravity measurements from the Gravity Recovery and Climate Experiment (GRACE) mission, altimetry, hydrography, and drifter data; while Colin de Verdière and Ollitrault (2016) estimated a strength of 124 Sv based on Argo float data. Several studies have pointed out that the strength of the ZA is highly variable, with strong interannual variability (e.g., Fu et al., 2001; Volkov and Fu, 2008; Saraceno et al., 2009; Yu et al., 2018; Venaille et al., 2011); an intra-seasonal mode of variability with a period of 25 days (Fu et al., 2001; Weijer et al., 2007a, b; Hughes et al., 2007; Yu et al., 2018); and even occasional collapses (Saraceno et al., 2009; Bigorre and Dewar, 2009).

The dynamics of the ZA was described by Dewar (1998). He explains how a seamount in an eddy-rich region leads to downslope transport of potential vorticity, and an associated upslope transport of mass. This mass convergence generates a high pressure dome over the seamount, which then forces an anticyclonic barotropic flow around it. Interestingly, the only mechanism to brake this flow is bottom drag; hence, the

* Corresponding author.
*E-mail address:* wilbert@lanl.gov (W. Weijer).
[1] now at Naval Postgraduate School, Monterey, CA.

https://doi.org/10.1016/j.dsr.2020.103308
Received 21 November 2019; Received in revised form 8 May 2020; Accepted 11 May 2020
Available online 5 July 2020

mass flux convergence in the interior water column is balanced by divergent Ekman transport in the bottom boundary layer. This picture was confirmed in numerical models by, for instance, de Miranda et al. (1999) and Volkov and Fu (2008). Weijer et al. (2015) recognized that this secondary circulation necessarily leads to downwelling motion within the vortex, and used an eddy-resolving ocean model to demonstrate that the downwelling transport increases almost linearly with depth. In fact, in their model, this process pumped no less than 4 Sv into the bottom Ekman layer; a staggering number given that the major overturning cells like the Atlantic Meridional Overturning Circulation involve less than 20 Sv of downwelling transports (e.g., Frajka-Williams et al., 2019).

The Argentine Basin is considered the main conduit for water mass exchanges between the Atlantic and Southern Oceans (e.g., Jullion et al., 2010). Given the strong vertical motions in the ZA, water masses transiting through the Argentine Basin may be affected by its dynamics. Yet, the impacts of the ZA on the large-scale ocean circulation remain largely unknown. This study takes a first step towards understanding the impacts of the ZA, by investigating its kinematics using Lagrangian particles in an eddy-permitting ocean model. Statistics on the evolution of the particles provide insight into the role the ZA may play in regional and large-scale circulation by supporting strong downwelling and water mass transformation.

## 2. Method

To examine the kinematics of the ZA, we use a Lagrangian approach to determine the fate of water parcels that start within the ZA. We use an offline particle tracking method, forced by velocity fields from an eddy-permitting ocean model. This 'parent' model is an ocean/sea ice standalone configuration of the E3SMv0-HiLAT model (Hecht et al., 2019), documented by Zhang et al. (2019). The model grid has a unique eddy-permitting resolution of 0.3°, and 100 levels in the vertical. This allows for a vigorous eddy field that reproduces the characteristic pattern in the Argentine Basin of high eddy kinetic energy surrounding a quiescent 'eye' over the Zapiola Rise, as observed by satellite altimetry (Zhang et al., 2019). No eddy parameterization is used, but a flux-limited advection scheme prevents numerical instabilities. The model was run for 186 years, forced by 3 cycles of CORE-II forcing (representing the historical period from 1948 to 2009). Our analysis window is a 5-year period starting from January 1 of year 98, for which 5-day averaged output was saved (temperature, salinity, and the 3 velocity components). The hydrographic properties over the Zapiole Rise compare well with observations (Fig. 2).

Figs. 3 and 4 show that the ZA is well represented in this model. Its mean strength of 112 Sv is close to the observational estimates of Saunders and King (1995a) and Colin de Verdière and Ollitrault (2016); also the variability is significant, with 5-daily values ranging between 50 and 246 Sv, consistent with observational estimates (e.g., Saraceno et al., 2009). The spectrum of the time series (Fig. 4b) is predominantly 'red' (Venaille et al., 2011), with significantly enhanced spectral energy at 25 days (Fu et al., 2001; Weijer et al., 2007a). This variability is also illustrated in Fig. 5, which shows snapshots of the barotropic stream function, in the context of its climatological mean. Fig. 2a clearly shows the strong downwelling within the ZA, which increases with depth; at 5100 m depth, it reaches 2 Sv, associated with an average downward velocity of about $8{\cdot}10^{-6}$ m/s. Below this depth, average vertical velocities increase even further, and reach values up to $26{\cdot}10^{-6}$ m/s when the water barrels down the flanks of the Zapiola Rise.

To track the fate of water parcels that start within the ZA, we use the Connectivity Modeling System (CMS; Paris et al., 2013). CMS calculates particle trajectories using velocity fields from a parent model. Here we use 5-day averaged velocity fields from E3SMv0-HiLAT. To determine our release locations, we first defined the ZA as the area enclosed by the

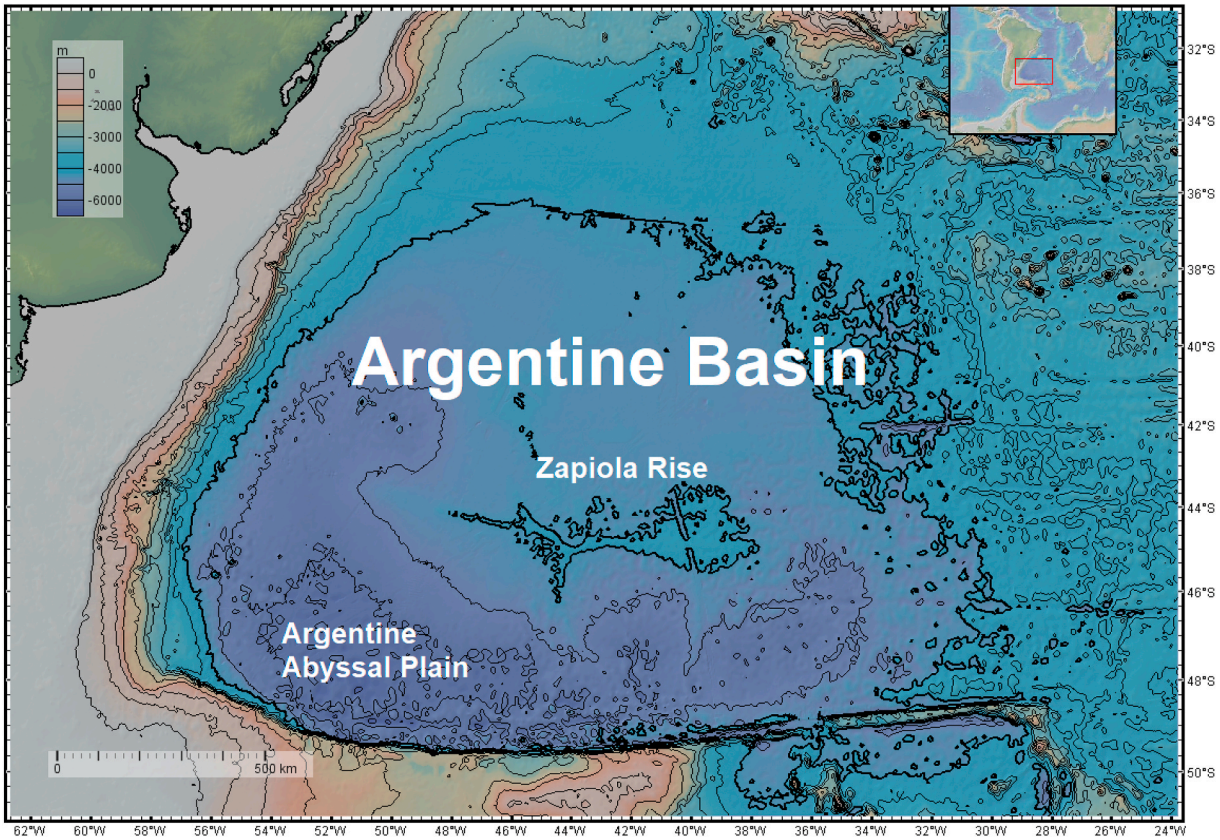


**Fig. 1.** Bathymetry of the Argentine Basin. Contour interval is 500 m, with the 5000 m isobath indicated in bold. Figure made with GeoMapApp (www.geomapapp.org; Ryan et al., 2009).

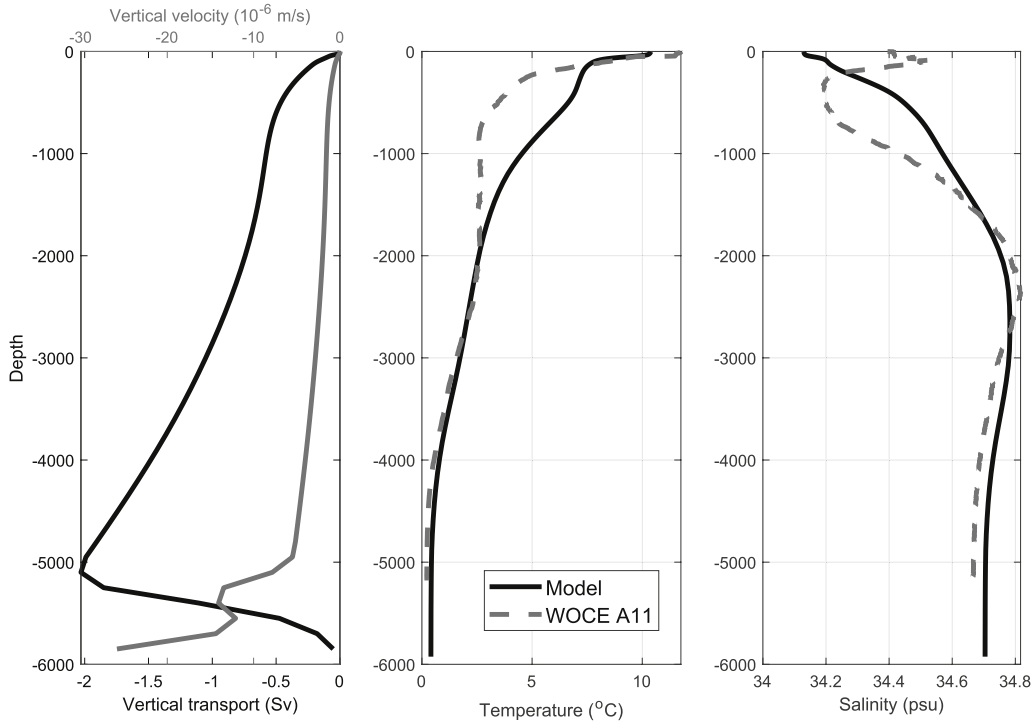


**Fig. 2.** a) Profile of net vertical transport (black) within the ZA; and profiles of a) vertical velocity (gray), b) potential temperature, and c) salinity, averaged over the ZA region. For reference, panels b) and c) show temperature and salinity profiles from station 12269 of the 1993 WOCE A11 cruise (44.7°W, 45.0°S; Saunders and King, 1995b).

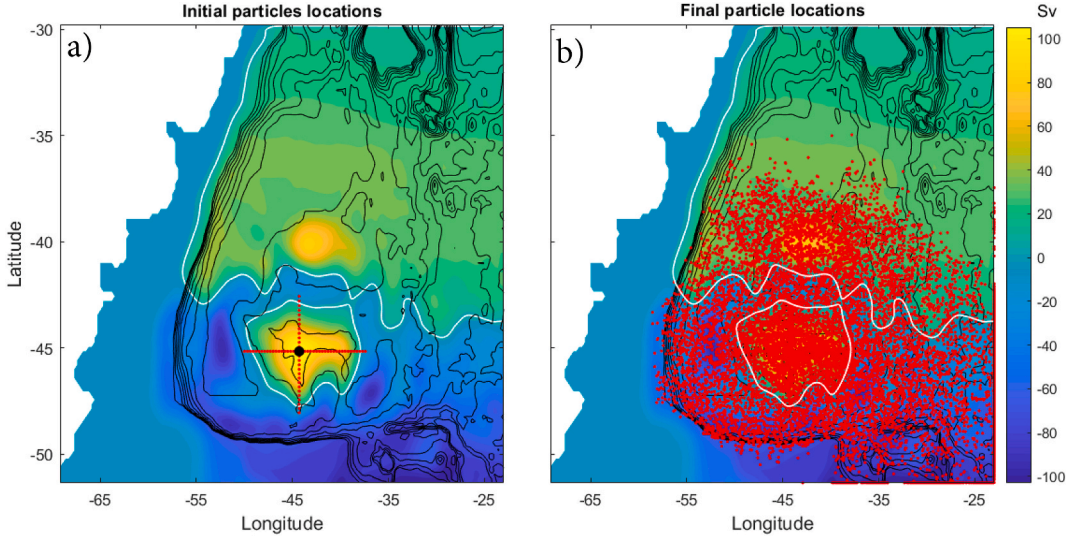


**Fig. 3.** a) Mean barotropic stream function (in Sv) for the Argentine Basin. White contour denotes the 5 Sv isoline that is used here to define the outline of the ZA. Black circle indicates the location of the maximum mean barotropic stream function (112 Sv) at 44.3°W, 45.2°S. The red symbols indicate the location of parcel releases. Contours of $f/H$ (black) are shown for bathymetric reference only. b) Same as a), but now showing the locations of the parcels at the end of the 5 year analysis period. Note that a subset of particles end up at the boundary of the analysis domain. (For interpretation of the references to color in this figure legend, the reader is referred to the Web version of this article.)

5 Sv contour of the mean barotropic stream function (white contour in Fig. 3a); and we designated the location of maximum mean barotropic stream function as the center of the ZA (black circle). We defined zonal and meridional release sections that intersect at the center of the ZA, and we released a particle for every 0.1° on the zonal and meridional release sections (red symbols), and at every 50 m depth between the surface and 6000 m depth. At $t = 0$, we released a total of 21,840 virtual particles. These particles were subjected to the integration algorithm in CMS, and a new location was determined every hour. The location of each particle was recorded every 5 days, and temperature and salinity were sampled at these locations and times. We followed the particles for 5 years, and the location of water parcels at the end of the 5-year analysis period is shown in Fig. 3b.

We found that of the 21,840 particles released, 2400 particles started outside the ZA (as we allowed the 'arms' of the release sections to extend slightly beyond the boundaries of the climatological ZA), while 1973 particles started out stuck on bathymetry, and were considered lost. So for our analysis we use the remaining 17,467 particles. We only consider

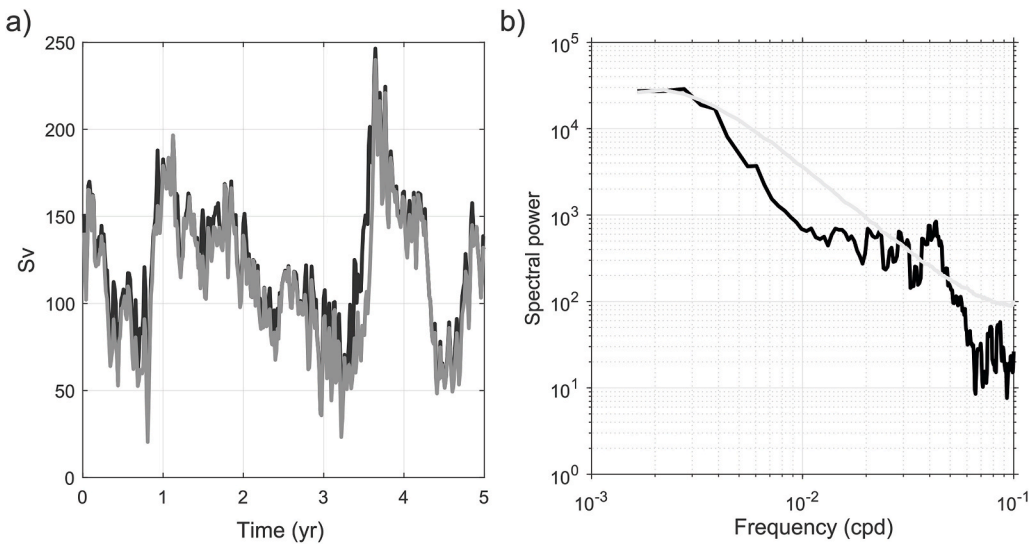


**Fig. 4.** a) Strength of the ZA for the 5 year analysis period. Black line is the ZA time series, defined as the maximum value of barotropic stream function within the ZA mask. Gray line is the stream function value at its climatological center (44.3°W, 45.2°S). b) Spectrum of the ZA time series. Light gray line is 90th percentile of 1000 synthetic time series with the same AR-1 characteristics as the ZA time series.

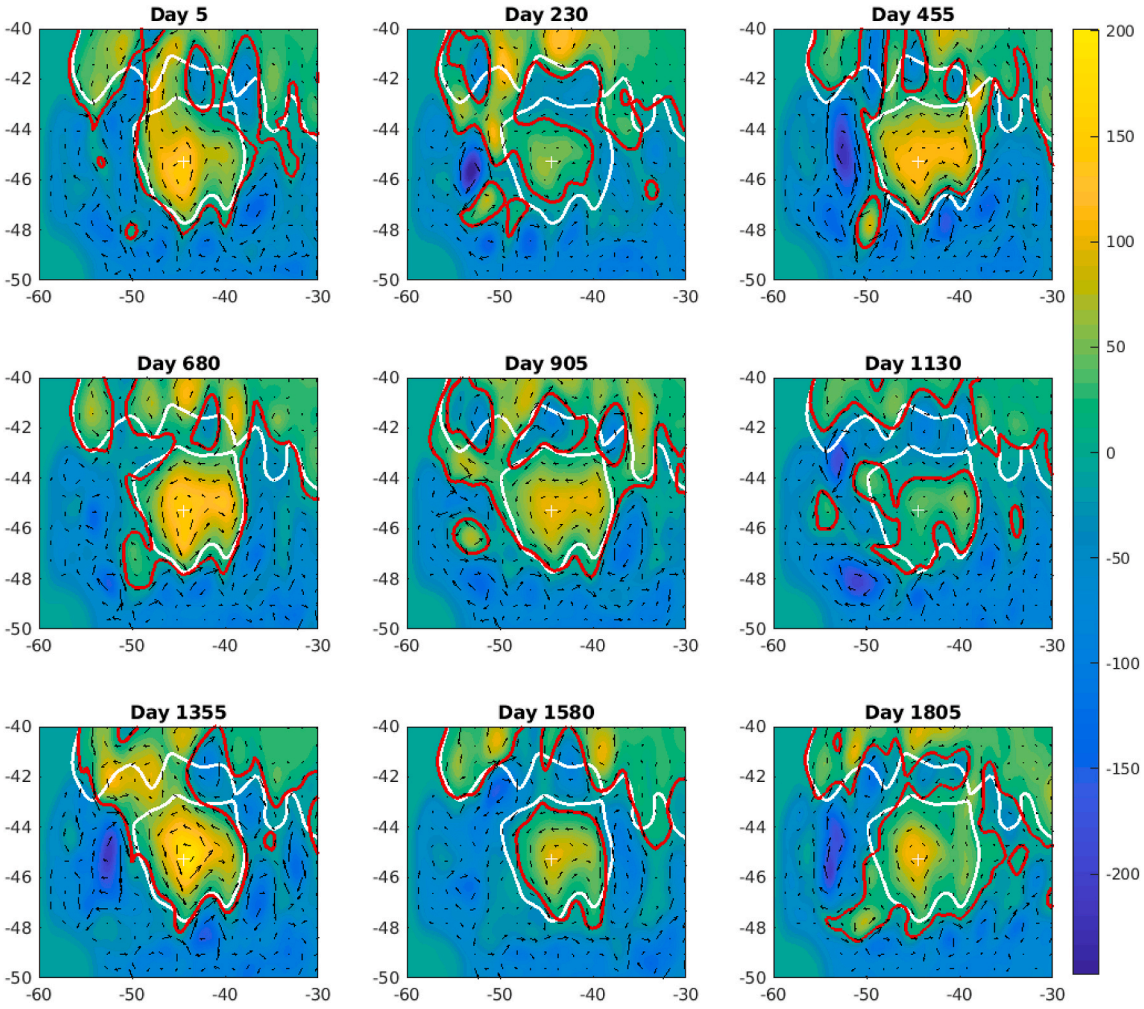


**Fig. 5.** A selection of 9 snapshots of 5-day averaged barotropic stream function. White line and plus-symbol indicates climatological position of the 5 Sv isoline that defines the ZA, and its center; while the red contour shows the instantaneous 5 Sv contour. Arrows indicate velocity vectors at 2000 m. (For interpretation of the references to color in this figure legend, the reader is referred to the Web version of this article.)

the particles trajectories until they leave the ZA for the first time. Also, we treat particles that get stuck on bathymetry during the simulation as if they have left the ZA. We deem a particle to be 'stuck' when it ceases to move horizontally. To calculate the number of revolutions of a parcel around the center of the ZA, we express its relative location with respect to the center of the ZA in polar coordinates $r(t),\varphi(t)$. Each time $\varphi(t)-\varphi_0$ crosses a multiple of 360°, the parcel is deemed to have completed another revolution.

In the next section we will explore several aspects of the water parcel trajectories from the moment of release at $t = 0$ until the moment of exit at $t = T_r$ (where $T_r$ is the retention time). Table 1 summarizes the statistics of several key metrics.

## 3. Results

### 3.1. Particle retention

First we explore the retention of the water parcels that started within the ZA. On average, parcels stay within the ZA for 451 days (Table 1). However, this average retention time increases from 115 days in the upper 1000 m to almost 2 years between 2000 and 3000 m. The retention curve (Fig. 6) shows that about 37% of the parcels is retained for at least a year, while 5% is still within the ZA at the end of the 5 year analysis period. The curve appears to display two time scales of decay, and can be accurately modeled by the sum of two exponential functions, with decay time scales of 180 (fast) and 800 (slow) days. Each decay mode contains roughly half of the particles.

Analysis of the retention time as function of release location (Fig. 7) suggests that the parcels with the shortest retention time are located in the upper 1000 m, and on the edges of the ZA. The fast mode therefore mostly consists of parcels that are released in the upper 1000 m, and are subjected to surface-intensified baroclinic circulation; and those on the edge of the ZA, which are most susceptible to eddies and meanders of the ZA (see Fig. 5). The slow mode consists of parcels that reside in the interior of the ZA and are isolated from surface currents or meanders of the ZA. However, this is not the complete story, as even closer to the center, and below 1000 m, there are clear regions where parcels are ejected quickly. These intricate patterns suggest that the processes that expel the parcels from the ZA may involve smaller scale exchanges between the ZA and its surroundings (as visible, for instance, in the instantaneous snapshots of barotropic stream function, Fig. 5).

**Table 1**
Key particle statistics, listed per depth range. Metrics are retention time $T_r$ (days), number of revolutions (#), time per revolution $T_l$ (days), vertical displacement $\Delta d$ (m), temperature change $\Delta T$ (°C), and salinity change $\Delta S$ ($10^{-3}$ psu). Shown are mean and standard error of the mean, with minimum and maximum values in brackets.

| Depth range | $T_r$ | # | $T_l$ | $\Delta d$ | $\Delta T$ | $\Delta S$ |
|---|---|---|---|---|---|---|
| 0–1000 m | 115 ± 2 | 0.69 ± 0.01 | 121 ± 2 | −22.2 ± 0.5 | 0.08 ± 0.01 | 18.1 ± 1.1 |
| | [0, 1370] | [-0.08, 7.48] | [25, 385] | [-178, 102] | [-2.91, 4.72] | [-140.3, 677.6] |
| 1000–2000 m | 316 ± 6 | 1.85 ± 0.03 | 151 ± 1 | −46 ± 1 | −0.04 ± 0.00 | 8.6 ± 0.2 |
| | [0, 1830] | [0.00, 14.59] | [15, 545] | [-287, 236] | [-0.78, 0.58] | [-36.6, 60.7] |
| 2000–3000 m | 502 ± 9 | 2.96 ± 0.05 | 154 ± 1 | −85 ± 2 | −0.04 ± 0.00 | 4.3 ± 0.2 |
| | [0, 1830] | [0.00, 14.74] | [15, 480] | [-578, 212] | [-0.51, 0.30] | [-30.7, 39.3] |
| 3000–4000 m | 699 ± 11 | 4.19 ± 0.07 | 156 ± 1 | −131 ± 3 | −0.12 ± 0.00 | −7.1 ± 0.1 |
| | [0, 1830] | [0.00, 17.72] | [15, 550] | [-695, 235] | [-0.58, 0.20] | [-37.6, 20.1] |
| 4000–6000 | 574 ± 8 | 3.10 ± 0.06 | 153 ± 1 | −161 ± 3 | −0.05 ± 0.00 | −3.3 ± 0.1 |
| | [0, 1830] | [-0.98, 17.28] | [15, 1590] | [-898, 344] | [-0.26, 0.09] | [-18.2, 6.4] |
| 0–6000 | 451 ± 4 | 2.60 ± 0.02 | 153 ± 0 | −94 ± 1 | −0.03 ± 0.00 | 4.2 ± 0.2 |

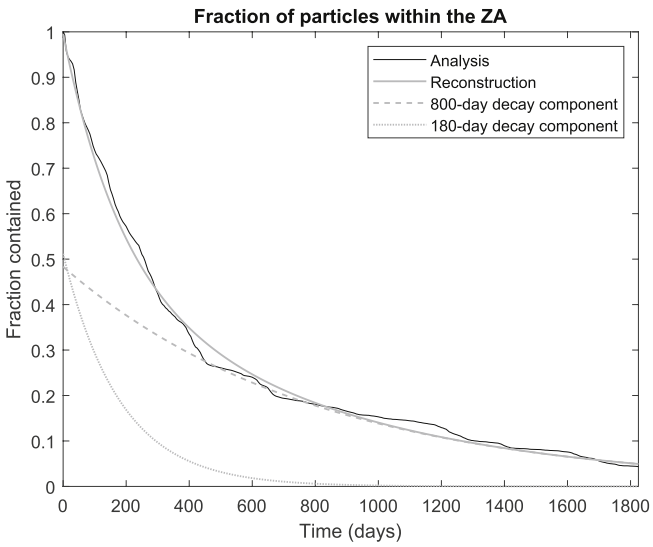


**Fig. 6.** Fraction of water parcels retained within the ZA as function of time. Parcel retention is modeled as a sum of two exponentials, with fast (180 days) and slow (800 day) decay time scales.

### 3.2. Loop statistics

While the parcels are being trapped by the ZA, they loop around its center on average 2.6 times (Table 1). Although more than 50% of the parcels are being ejected before completing 1.5 revolutions, 20% completes 3.5 revolutions or more, roughly 10% completes more than 7.5 revolutions, and some undergo as many as 18 revolutions. The ability to hang around longer increases with depth, as shown by Fig. 8a. For the top layer, less than 1% of the parcels hang around long enough to complete 3.5 revolutions or more, while this is 42% for the 3000–4000 m depth range. The deepest bin (> 4000 m) is atypical: it has a long tail like the other deep bins, but a high peak at zero revolutions. This likely reflects the lower retention time of deep parcels (Fig. 7), due to the strong divergent circulation in the bottom boundary layer.

The time it takes for parcels to complete a revolution ($T_l$) is shown in Fig. 8b. Average revolution time is 153 days (Table 1), but times of 200 days or longer are not uncommon. For depths below 2000 m, the distributions have a bimodal character, with preferred modes of 100 and 175 days. The reason for this bimodality is the fact that the ZA is strongest over the western part of the Zapiola Rise, while weaker circulation extends over the eastern part (Figs. 3 and 5). One might argue that this western intensification represents a stronger sub-cell within the ZA proper. The parcels that go around the entire ZA experience revolution times that are significantly longer than parcels that circulate within the western cell only. Note that this bimodality is not seen for parcels released above 2000 m depth, possibly due to the stronger influence of the baroclinic circulation not associated with the ZA. Note that, although the fraction of parcels that start in each of the 5 depth bins is approximately the same (20%), the parcels that are released in the deeper bins make more revolutions (see Fig. 8, left panel), giving us larger sample sizes for the deeper bins.

### 3.3. Ejection direction

While the ZA can retain parcels for several years (Section 3.1), the fate of water exiting the ZA determines its influence on the surrounding region. Thus, it is important to determine what the preferential exit

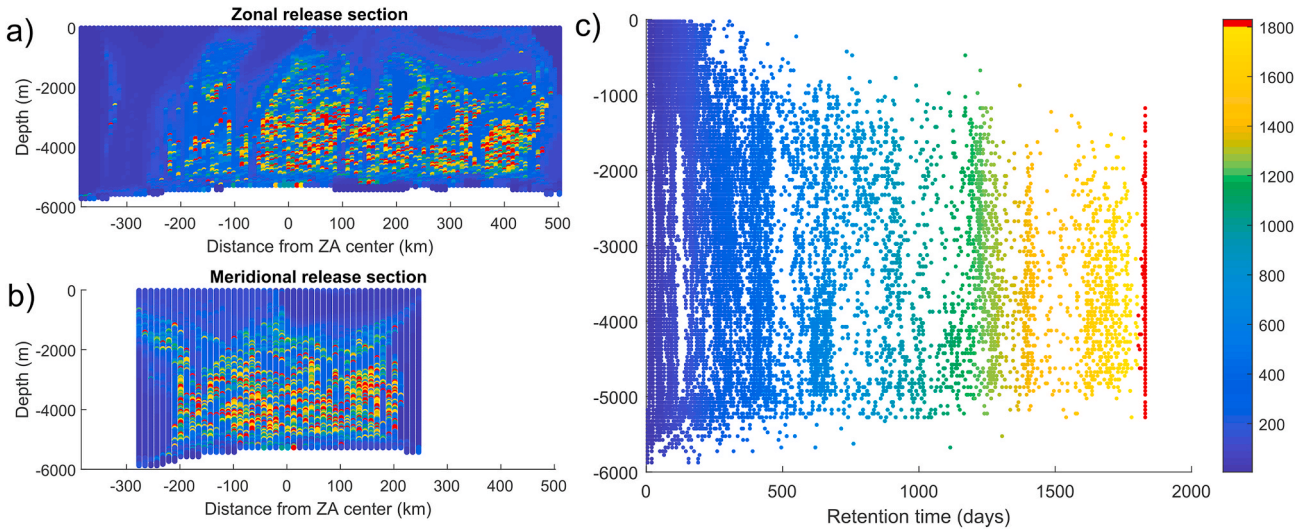


**Fig. 7.** Retention time (days) as function of release location on the a) zonal and b) meridional release section, and c) as function of depth of release. Red dots indicate parcels that have not left the ZA at the end of the analysis period. (For interpretation of the references to color in this figure legend, the reader is referred to the Web version of this article.)

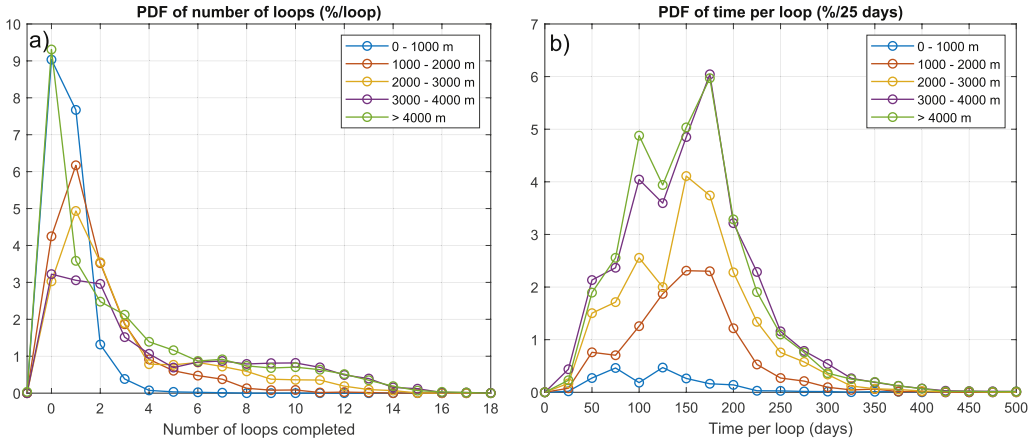


**Fig. 8.** Probability Density Functions (PDFs) of a) the number of revolutions before the parcels are ejected from the ZA, and b) the time per revolution. In each case, the parcels are binned by depth of release, as indicated in the legend.

locations (in both depth and direction) are around the perimeter of the ZA. Fig. 9 show that parcels preferably exit the ZA to the east and southeast (35%), while the lowest fraction of parcels exit to the north or northwest (16%). The directional preference changes somewhat with depth, as the east-southeastward dominance is particularly strong for parcels that exit the ZA in the deepest bin (deeper than 4000 m); while above 2000 m, the preferred exit direction is south-southeastward.

The directional preference is quite consistent with the results from Saraceno and Provost (2012). They analyze pathways of eddies in the Argentine Basin, and find that eddies that enter the ZA do so mainly on the eastern side. They argue that the gradient of barotropic potential vorticity $f/H$ is weakest on the eastern side of the Zapiola Rise, giving the ZA more opportunity to meander there than on the sides where the gradient is stronger. Saraceno and Provost (2012) suggest that meanders of the ZA can turn into cyclonic eddies inside the ZA, and anticyclonic eddies outside, especially during periods of low ZA strength. So this provides a mechanism for enhanced exchanges between the ZA and its surroundings. The tendency for exit directions to turn more southward at shallower levels may reflect the increasing influence of the baroclinic circulation not related to the ZA: the potential vorticity barrier is probably strongest on the north side of the Zapiola Rise, where a strong gradient exists between the eastward flowing South Atlantic Current and the westward flow at the northern rim of the ZA; on the south the eastward circulation along the subpolar front is in the same direction as the southern limb of the ZA, making it easier for parcels to escape.

### 3.4. Vertical displacement, property changes

The previous sections show that the ZA has the ability to retain water parcels for many years. But while being trapped, the parcels also undergo a mostly downward displacement ($\Delta d$), and associated changes in temperature ($\Delta T$) and salinity ($\Delta S$; Fig. 10; Table 1). For all depth bins, the Probability Density Functions (PDFs) show a peak at zero vertical displacement (except for 1000–2000 m bin, which peaks at −50 m). But the distributions are clearly skewed towards negative displacements, with the tails of the distributions becoming longer for the deeper bins. In fact, average vertical displacement exceeds −100 m below 3000 m, but downward displacements can be as much as 800 m. On average the parcels undergo a cooling of 0.03 °C (0.06 °C below 1000 m) as they move through the background stratification (Fig. 2). The salinity changes are more complex, as water parcels originating in the relatively fresh upper layer become saltier as they enter the high-salinity North Atlantic Deep Water (NADW); while parcels starting within the NADW layer become fresher as they mix into the Antarctic Bottom Water

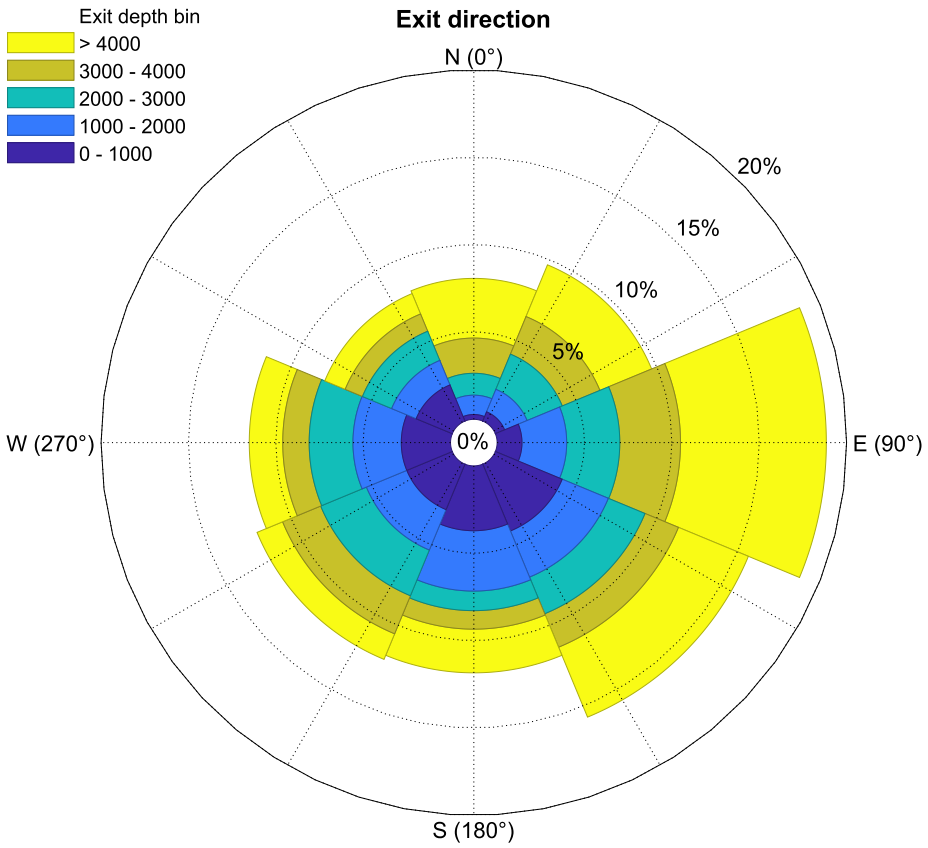


**Fig. 9.** Direction in which particles exit the ZA, binned by depth of their exit.

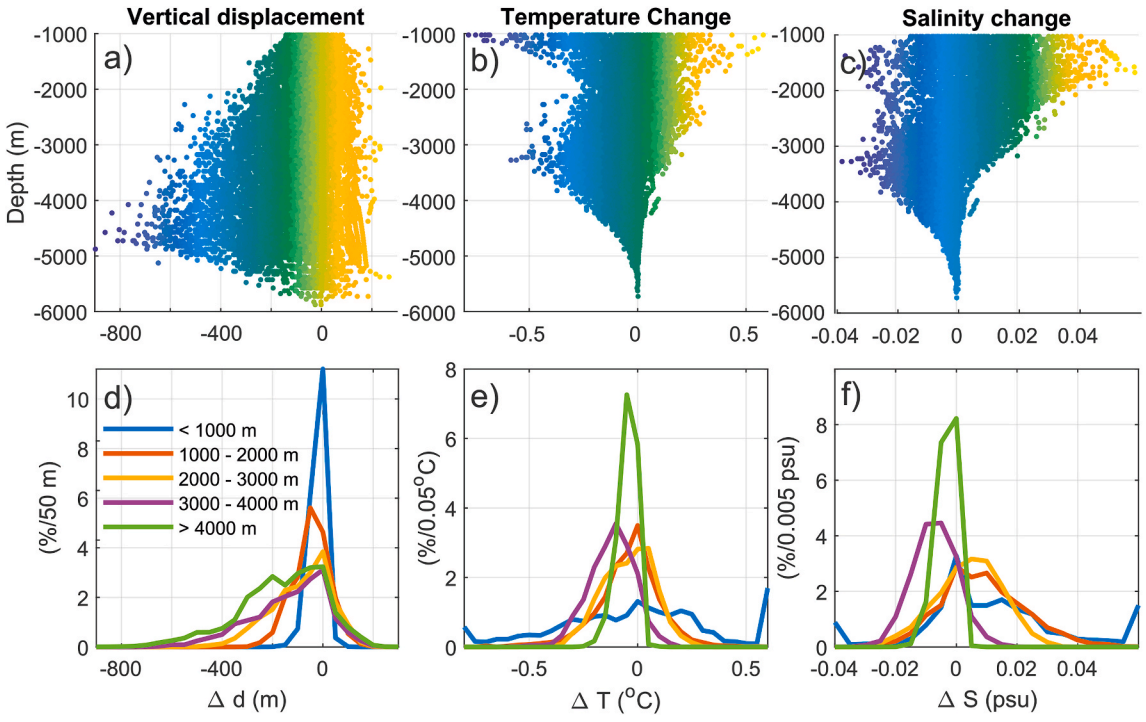


**Fig. 10.** Net changes in a) depth ($\Delta d$), b) temperature ($\Delta T$), and c) salinity ($\Delta S$), at the time particles exit the ZA, shown as function of their release depth (below 1000 m). Symbol coloring is for visual guidance only. Associated PDFs for 5 depth bins are shown in panels d–f.

(AABW).

To explore the diapycnal and isopycnal transformations of the water parcels, we calculate the thermal ($\sigma_T = -\alpha\Delta T$) and haline ($\sigma_S = \beta\Delta S$) contributions to the potential density changes ($\sigma_2$, defined with respect to 2000 dbar), where α and β are thermal and haline coefficients of expansion. In particular, we separate $\sigma_T$ into a component that is

compensated by salinity changes ($\sigma_{T,C} = -\sigma_S$), and a remainder that is uncompensated ($\sigma_{T,U} = \sigma$). Fig. 11 shows that the parcels undergo both diapycnal and isopycnal transformations. The density changes are clearly skewed positive, consistent with cooling of descending particles (Fig. 2a and b). The density-compensated changes are generally smaller, consistent with the thermal dominance of the stratification. The density-compensated changes are consistent with the salinity profile shown in Fig. 2c, which shows a maximum at 2500 m depth. The changes are skewed negative above 2500 m, where downwelling motion is associated with salinification (Fig. 2c); while below 2500 m downwelling is associated with freshening.

Both the isopycnal and diapycnal transformations of the water parcels during their (mostly) downward motion reflect the action of mixing processes, but it is not clear how this relates to the overall buoyancy budget of the ZA. Here we attempt to reconcile our Lagrangian perspective with a Eulerian view, realizing that our experimental set-up –a single release of parcels starting within the ZA– is not well-suited for quantifying exchange processes between the ZA and its surroundings. First, Fig. 12 shows that the time-mean horizontal velocity field above 5000 m is convergent (Fig. 12a), is balanced by the divergence of vertical transport, and compensated by net divergence in the bottom boundary layer below 5000 m. This is consistent with Fig. 2a and our theoretical understanding of the dynamics of the ZA (Dewar, 1998). Fig. 12 b-d show that this mean circulation leads to a divergent density flux (black dashed), as buoyant (warmer and generally fresher) water is pumped into the ZA, transported downward, and exported at denser (colder and saltier) levels. This process is largely counterbalanced by convergent horizontal eddy fluxes of density (dotted blue). Vertical eddy transport is negligibly small (dotted red). The residual (solid black) is small but slightly positive, indicating that the explicitly resolved processes tend to converge buoyancy (dominated by heat). Unresolved processes like vertical mixing, and implicit diffusion associated with the flux-limited advection scheme, must hence provide a sink of buoyancy to close the budget. So we speculate that the diapycnal processes responsible for the density changes of the descending water parcels inside the ZA are a result of diffusive lateral exchanges with the surrounding waters, and only represent a small component of the overall buoyancy budget of the ZA, which is dominated by a balance between horizontal eddy fluxes and the mean flow.

## 4. Discussion and conclusion

In this paper we analyze the fate of water within the ZA, by modeling water parcels as Lagrangian particles and tracking their fate as they are being advected by the variable circulation of the ZA. The picture that emerges is of water parcels spiraling downward within the ZA, undergoing significant downwelling while making several revolutions around the center of the ZA. This is illustrated by Fig. 13, which shows the trajectory of one individual water parcel. This parcel starts at a depth of 4700 m and exits the ZA 840 m deeper, at 5540 m. It spends 3 years and 7 months within the ZA, and undergoes 6.6 revolutions. On average, in our experiment, water parcels spend 451 days within the ZA, make 2.6 revolutions around its center, undergo a 94 m descend, and experience 0.03° cooling and 0.0042 psu freshening.

The vertical motions associated with this downwelling are of the order of $10 - 20{\cdot}10^{-6}$ m/s at depths below 5000 m (Fig. 2). To put these numbers in perspective, these velocities are larger than typical surface Ekman pumping velocities in the mid-latitude oceans ($5{\cdot}10^{-6}$ m/s; Risien and Chelton, 2008), and are on par with estimates of vertical velocities in some coastal upwelling zones (e.g., Steinfeldt et al., 2015). Other processes with large vertical displacements are the deep and bottom water formation at high latitudes. Katsman et al. (2018) analyze vertical velocities and transports associated with the Atlantic overturning circulation in the subpolar North Atlantic, using a model in two different configurations; one of which has an 0.25° eddy-permitting spatial resolution. They show that most of the downwelling takes place in the western boundary current. Typical downward velocities along the shelf are on the order of 30 m/day, or $3.5{\cdot}10^{-4}$ m/s; hence an order of magnitude larger than the vertical velocities within the ZA. Still, these processes are strongly tied to continental topography. We are not aware of any other process that generates such strong downwelling motions in the abyssal mid-latitude oceans.

A question raised by this analysis is the extent to which the water mass transformations in the ZA affect the hydrography of the Argentine Basin, and the stratification of the South Atlantic Ocean in general. This is a difficult problem to address using the current Lagrangian approach, and we will leave a proper quantification of its impact for further study with more appropriate methodologies. But it is interesting to note that parcels released within the ZA are dispersed over both the subpolar and subtropical sectors of the southwest South Atlantic Ocean (Fig. 3b); and given that the Argentine Basin is a cauldron where several of the ocean's major water masses meet (Jullion et al., 2010), further investigation of the regional and large-scale impacts of the ZA is warranted.

The study shows that our ocean model with 0.3° spatial resolution and 100 vertical levels ably captures the eddy-driven dynamics of the ZA. In fact, the model appears to represent the strength of the ZA more

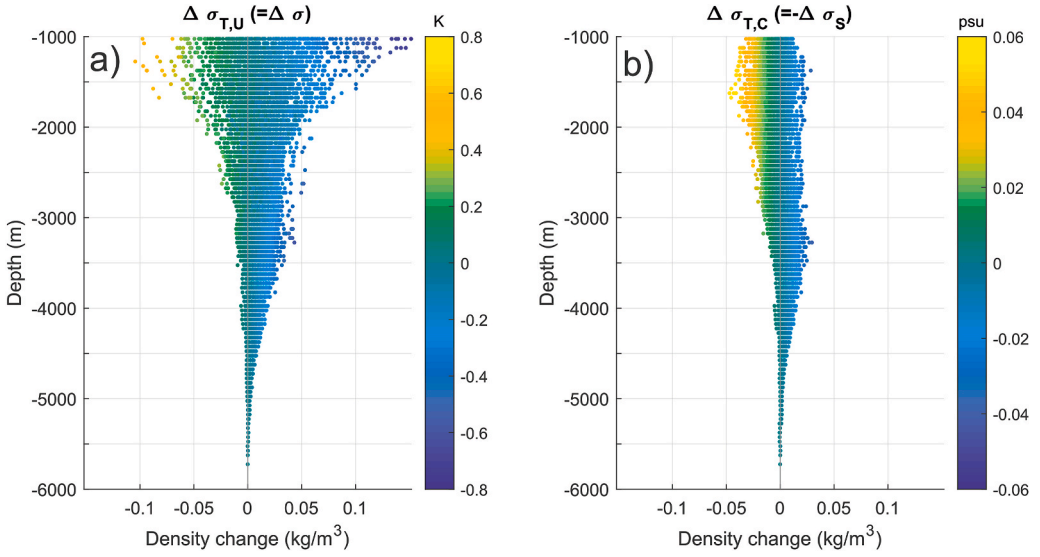


**Fig. 11.** Thermal contributions to density changes experienced by parcels in the ZA: a) uncompensated thermal density changes; b) thermal density changes that are compensated by salinity changes. Color coding represents temperature ($\Delta T$) and salinity $\Delta S$ changes, respectively. Thermal (α) and haline (β) expansion coefficients are determined using the Gibbs-SeaWater (GSW) Oceanographic Toolbox for Matlab, and referenced to 2000 dbar (McDougall and Barker, 2011). (For interpretation of the references to color in this figure legend, the reader is referred to the Web version of this article.)

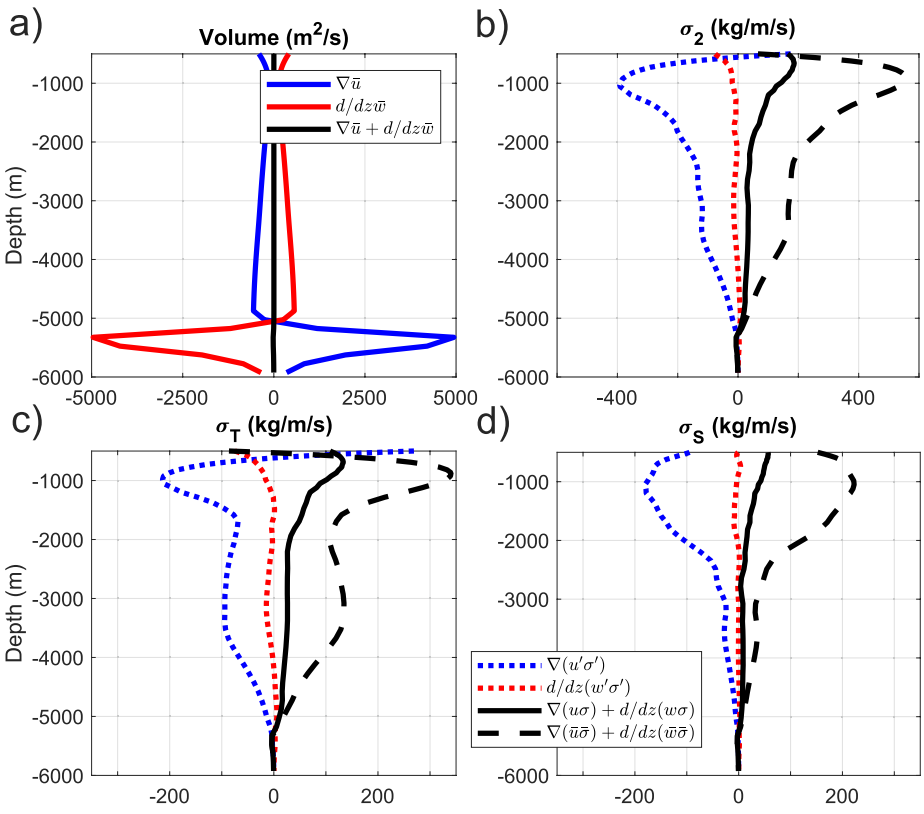


**Fig. 12.** Budgets of the ZA, plotted as flux divergences integrated over the ZA region. Shown are a) divergence of the 3D velocity field (black), and its horizontal (blue) and vertical (red) components; b) divergence of 3D advective fluxes of potential density ($\sigma_2$; black), its time-mean contributions (black dashed), and the horizontal (blue) and vertical (red) eddy components; c) and d) as b), but now for the thermal ($\sigma_T$) and haline ($\sigma_S$) contributions to $\sigma_2$. We define $\sigma_T = -\alpha T$ and $\sigma_S = \beta S$, where thermal (α) and haline (β) expansion coefficients are determined using the Gibbs-SeaWater (GSW) Oceanographic Toolbox for Matlab (McDougall and Barker, 2011), referenced to 2000 dbar, and after proper conversion from potential to conservative temperature. We remove the volume- and time-mean values of $\sigma_T$ and $\sigma_S$ before calculating the advective transports, and define $\sigma_2 = \sigma_T + \sigma_S$. (For interpretation of the references to color in this figure legend, the reader is referred to the Web version of this article.)

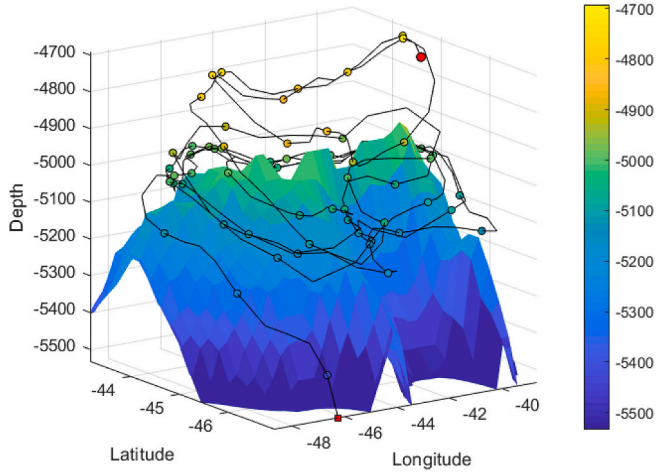


**Fig. 13.** Trajectory of a single water parcel. A symbol is plotted every 20 days, with marker color indicating depth; and its start and end positions are indicated by a red circle and square, respectively. (For interpretation of the references to color in this figure legend, the reader is referred to the Web version of this article.)

accurately than a configuration of the same base model with eddy-resolving (0.1°) resolution and 42 levels (Weijer et al., 2015), which simulated a mean ZA strength of no less than 270 Sv. Indeed, Barnier et al. (2006) shows how the representation of the ZA is very sensitive to details of a model's numerics, and that other factors than horizontal resolution may be decisive in whether a model features a realistic ZA or not. It would be illustrative to compare the particle statistics between different models to test the robustness of the results reported here.

## Declaration of competing interest

The authors declare that they have no known competing financial interests or personal relationships that could have appeared to influence the work reported in this paper.

## Acknowledgements

This research was supported by the Regional and Global Model Analysis (RGMA) component of the Earth and Environmental System Modeling (EESM) program of the U.S. Department of Energy's Office of Science. Hannah Steiner was supported by the Service Academies Research Associates (SARA) program of Los Alamos National Laboratory. We would like to thank the Editor and 3 anonymous Reviewers for their thoughtful comments, and we acknowledge stimulating conversations with Bill Dewar (Florida State University) and Will de Ruijter (Utrecht University).

## References

Barnier, B., Madec, G., Penduff, T., Molines, J.M., Treguier, A.M., Le Sommer, J., Beckmann, A., Biastoch, A., Böning, C., Dengg, J., et al., 2006. Impact of partial steps and momentum advection schemes in a global ocean circulation model at eddy-permitting resolution. Ocean Dynam. 56, 543–567. https://doi.org/10.1007/s10236-006-0082-1.

Bigorre, S., Dewar, W.K., 2009. Oceanic time variability near a large scale topographic circulation. Ocean Model. 29, 176–188. https://doi.org/10.1016/j.ocemod.2009.04.004.

Colin de Verdière, A., Ollitrault, M., 2016. A direct determination of the World Ocean barotropic circulation. J. Phys. Oceanogr. 46, 255–273. https://doi.org/10.1175/JPO-D-15-0046.1.

de Miranda, A.P., Barnier, B., Dewar, W.K., 1999. On the dynamics of the Zapiola Anticyclone. J. Geophys. Res.: Oceans 104, 21137–21149. https://doi.org/10.1029/1999JC900042.

Dewar, W.K., 1998. Topography and barotropic transport control by bottom friction. J. Mar. Res. 56, 295–328. https://doi.org/10.1357/002224098321822320.

Frajka-Williams, E., Ansorge, I.J., Baehr, J., Bryden, H.L., Chidichimo, M.P., Cunningham, S.A., Danabasoglu, G., Dong, S., Donohue, K.A., Elipot, S., et al., 2019.

Atlantic meridional overturning circulation: observed transports and variability. Front. Mar. Sci. 6, 260. https://doi.org/10.3389/fmars.2019.00260.
Fu, L.L., Cheng, B., Qiu, B., 2001. 25-day period large-scale oscillations in the Argentine Basin revealed by the TOPEX/Poseidon altimeter. J. Phys. Oceanogr. 31, 506–517. https://doi.org/10.1175/1520-0485(2001)031<0506:DPLSOI>2.0.CO;2.
Hecht, M., Veneziani, M., Weijer, W., Kravitz, B., Comeau, D., Hunke, E., Jeffery, N., Wang, H., Wang, S., Zhang, J., Mills, C., Rasch, P., Urban, N., 2019. E3SMv0-HiLAT: a modified climate system model targeted for the study of high-latitude processes. J. Adv. Model. Earth Syst. 11 https://doi.org/10.1029/2018MS001524.
Hughes, C., Stepanov, V., Fu, L.L., Barnier, B., Hargreaves, G., 2007. Three forms of variability in Argentine Basin ocean bottom pressure. J. Geophys. Res.: Oceans 112. https://doi.org/10.1029/2006JC003679.
Jullion, L., Heywood, K.J., Naveira Garabato, A.C., Stevens, D.P., 2010. Circulation and water mass modification in the Brazil–Malvinas Confluence. J. Phys. Oceanogr. 40, 845–864. https://doi.org/10.1175/2009JPO4174.1.
Katsman, C.A., Drijfhout, S., Dijkstra, H.A., Spall, M.A., 2018. Sinking of dense North Atlantic waters in a global ocean model: location and controls. J. Geophys. Res.: Oceans 123, 3563–3576. https://doi.org/10.1029/2017JC013329.
McDougall, T.J., Barker, P.M., 2011. Getting started with TEOS-10 and the Gibbs Seawater (GSW) oceanographic toolbox. SCOR/IAPSO WG 127, 1–28.
Paris, C.B., Helgers, J., Van Sebille, E., Srinivasan, A., 2013. Connectivity Modeling System: a probabilistic modeling tool for the multi-scale tracking of biotic and abiotic variability in the ocean. Environ. Model. Software 42, 47–54. https://doi.org/10.1016/j.envsoft.2012.12.006.
Rio, M., Schaeffer, P., Hernandez, F., Lemoine, J., 2005. The estimation of the ocean Mean Dynamic Topography through the combination of altimetric data, in-situ measurements and GRACE geoid: from global to regional studies. In: Proceedings of the GOCINA International Workshop, Luxembourg.
Risien, C.M., Chelton, D.B., 2008. A global climatology of surface wind and wind stress fields from eight years of QuikSCAT scatterometer data. J. Phys. Oceanogr. 38, 2379–2413. https://doi.org/10.1175/2008JPO3881.1.
Ryan, W.B.F., Carbotte, S.M., Coplan, J.O., O'Hara, S., Melkonian, A., Arko, R., Weissel, R.A., Ferrini, V., Goodwillie, A., Nitsche, F., Bonczkowski, J., Zemsky, R., 2009. Global multi-resolution topography synthesis. G-cubed 10. https://doi.org/10.1029/2008GC002332.
Saraceno, M., Provost, C., 2012. On eddy polarity distribution in the southwestern Atlantic. Deep Sea Res. Oceanogr. Res. Pap. 69, 62–69. https://doi.org/10.1016/j.dsr.2012.07.005.
Saraceno, M., Provost, C., Zajaczkovski, U., 2009. Long-term variation in the anticyclonic ocean circulation over the Zapiola Rise as observed by satellite altimetry: evidence of possible collapses. Deep Sea Res. Oceanogr. Res. Pap. 56, 1077–1092. https://doi.org/10.1016/j.dsr.2009.03.005.
Saunders, P.M., King, B.A., 1995a. Bottom currents derived from a shipborne ADCP on WOCE cruise A11 in the South Atlantic. J. Phys. Oceanogr. 25, 329–347. https://doi.org/10.1175/1520-0485(1995)025<0329:BCDFAS>2.0.CO;2.
Saunders, P.M., King, B.A., 1995b. Oceanic fluxes on the WOCE A11 section. J. Phys. Oceanogr. 25, 1942–1958. https://doi.org/10.1175/1520-0485(1995)025<1942:OFOTWA>2.0.CO;2.
Steinfeldt, R., Sültenfuß, J., Dengler, M., Fischer, T., Rhein, M., 2015. Coastal upwelling off Peru and Mauritania inferred from helium isotope disequilibrium. Biogeosciences 12, 7519–7533. https://doi.org/10.5194/bg-12-7519-2015.
Venaille, A., Le Sommer, J., Molines, J.M., Barnier, B., 2011. Stochastic variability of oceanic flows above topography anomalies. Geophys. Res. Lett. 38 https://doi.org/10.1029/2011GL048401.
Volkov, D.L., Fu, L.L., 2008. The role of vorticity fluxes in the dynamics of the Zapiola Anticyclone. J. Geophys. Res.: Oceans 113. https://doi.org/10.1029/2008JC004841.
Weijer, W., Vivier, F., Gille, S.T., Dijkstra, H.A., 2007a. Multiple oscillatory modes of the Argentine Basin. Part I: statistical analysis. J. Phys. Oceanogr. 37, 2855–2868. https://doi.org/10.1175/2007JPO3527.1.
Weijer, W., Vivier, F., Gille, S.T., Dijkstra, H.A., 2007b. Multiple oscillatory modes of the Argentine Basin. Part II: the spectral origin of basin modes. J. Phys. Oceanogr. 37, 2869–2881. https://doi.org/10.1175/2007JPO3688.1.
Weijer, W., Maltrud, M.E., Homoky, W.B., Polzin, K.L., Maas, L.R., 2015. Eddy-driven sediment transport in the Argentine Basin: is the height of the Zapiola Rise hydrodynamically controlled? J. Geophys. Res.: Oceans 120, 2096–2111. https://doi.org/10.1002/2014JC010573.
Yu, Y., Chao, B.F., García-García, D., Luo, Z., 2018. Variations of the Argentine Gyre observed in the GRACE time-variable gravity and ocean altimetry measurements. J. Geophys. Res.: Oceans 123, 5375–5387. https://doi.org/10.1029/2018JC014189.
Zhang, J., Weijer, W., Maltrud, M.E., Veneziani, C., Jeffery, N., Hunke, E.C., Urrego Blanco, J.R., Wolfe, J.D., 2019. An Eddy-Permitting Ocean-Sea Ice General Circulation Model (E3SMv0-HiLAT03): Description and Evaluation. Technical Report. Los Alamos National Lab.(LANL), Los Alamos, NM (United States). https://doi.org/10.2172/1542803.